Article
Real-Driving Emissions of an Aging Biogas-Fueled City Bus

Kirsi Spoof-Tuomi [1],*, Hans Arvidsson [2] , Olav Nilsson [1] and Seppo Niemi [1]

[1] School of Technology and Innovations, University of Vaasa, Box 700, FI-65101 Vaasa, Finland
[2] RISE Research Institutes of Sweden, Box 5053, SE-90403 Umeå, Sweden
*   Correspondence: kirsi.spoof-tuomi@uwasa.fi

Abstract: Transition to low emission transportation and cleaner cities requires a broad introduction of low- and zero-carbon alternatives to conventional petrol- and diesel-powered vehicles. New-generation gas buses are a cost-effective way to reduce local air pollutants from urban transportation. Moreover, major greenhouse gas (GHG) savings may be achieved using biogas as the power source. The main objective of this research was to investigate CH_4 and other gaseous emissions of a biogas-fueled urban bus equipped with a three-way catalyst (TWC) in real-world conditions. The study focused on emissions from a six-year-old gas-powered city bus, supplementing emission data from aging bus fleets. Impaired CH_4 oxidation and NO_x reduction were observed in the catalyst after its service life of 375,000 km–400,000 km. The main reason for low CH_4 and NO_x conversion over the TWC was concluded to be the partial deactivation of the catalyst. Another critical issue was the fluctuating air-to-fuel ratio. The results show that the efficiency of exhaust after-treatment systems should be closely monitored over time, as they are exposed to various aging processes under transient driving conditions, leading to increased real-world emissions. However, the well-to-wheels (WTW) analysis showed that an 80% GHG emission benefit could be achieved by switching from diesel to biomethane, giving a strong environmental argument for biogas use.

Keywords: real-driving emission; portable emission measurement system; Euro VI; urban bus; catalyst deactivation; compressed biogas; well-to-wheels analysis

1. Introduction

There is a worldwide consensus that significant reductions in greenhouse gas (GHG) emissions are needed to avoid the worst impacts of climate change, and various laws and regulations have already been implemented to combat and respond to global warming. In July 2021, the European Commission adopted an extensive legislative package, Fit for 55, with the goal of reducing the economy-wide GHG emissions by at least 55% by 2030 compared to 1990 levels [1]. This is a substantial increase from the previous 40% target. Achieving the 55% reduction in GHG emissions over the next decade is crucial for Europe to achieve climate neutrality by 2050. Moreover, Finland has set itself the goal of becoming carbon neutral by 2035 [2]. This is one of the most ambitious targets of any country in the industrialized world.

In 2019, GHG emissions from domestic transportation accounted for 21 percent of Finland's total greenhouse gas emissions and about 30 percent of the energy sector's GHG emissions [3]. Road transportation is likely to remain a significant contributor to air pollution in the coming decades, especially in urban areas [4]. Transition to low emission transportation and cleaner cities will undoubtedly require a broad introduction of low- and zero-carbon alternatives to conventional petrol- and diesel-powered vehicles.

New generation gas buses are a cost-effective way to reduce CO_2 and local pollutants from urban transportation. Fueling with gas reduces pollutant emissions, including carbon monoxide (CO), nitrogen oxides (NO_x), and particulate matter (PM), as shown, e.g., by Biernat et al. [5]. Moreover, major GHG savings can be achieved by using biogas as the power source. This is based on the fact that producing biomethane from organic waste

material results in fuel that contains only biogenic carbon, and combustion of such fuel releases only biogenic CO_2, which is, unlike CO_2 from fossil fuels, not considered to contribute the climate change [6].

Buses running on biogas are becoming more common in Finland as cities and transportation companies invest in greener alternatives. For example, in the western coastal city of Vaasa, biogas buses have been touring since 2017. Life cycle GHG emissions from biogas vehicles largely depend on the extent of methane (CH_4) leakage throughout the fuel life cycle, and unintended CH_4 emissions from different stages of the fuel chain can narrow their potential climate benefits. Methane is a powerful greenhouse gas with a global warming potential (GWP) 28–34 times that of CO_2 over a 100-year timescale [7]. In addition, due to the strong C–H bonds of methane, it is one of the most difficult hydrocarbons to treat catalytically [8], and insufficient removal rates of exhaust after-treatment systems at low loads and low exhaust temperatures may lead to increased real-world CH_4 emissions [9].

Besides exhaust gas temperature, another critical issue is the effect of rapid changes in exhaust gas composition—typical in real-world driving conditions—on after-treatment devices. This phenomenon is particularly evident when dealing with stoichiometric gas engines using three-way catalytic converters (TWC), requiring a very precise control of air-to-fuel ratio (AFR), as some deviations from the stoichiometric lambda value can interfere with the catalyst efficiency [10]. For example, Rodman Oprešnik et al. [11] reported instantaneous, local rises of THC emissions as a result of occasional inadequate lambda control of a CNG bus during transient regime and, consequently, increased cumulative emissions.

The main objective of this research was to investigate CH_4 and other gaseous emissions plus fuel consumption of a biogas-fueled urban bus in real-world operation. The actual driving emissions were recorded using a portable emissions measurement system (PEMS). The key advantage of on-board measurements is that they can truly demonstrate the emission characteristics of vehicles under various traffic conditions, operating cycles, and ambient conditions, including those that are challenging to replicate in the laboratory, such as varying road gradients [4]. The load on the lines that buses serve and the number of passengers may also affect exhaust emissions under actual traffic conditions [12].

Exhaust emissions under real-world conditions were examined by Lv et al. [13]. The authors showed an underestimation of road emissions of gas- and diesel-powered heavy vehicles; emission factors under real-driving conditions were significantly higher than in previous chassis dynamometer studies, likely caused by frequent accelerations, decelerations, and start-stop operation. In a recent study, Rosero et al. [14] investigated the effects of passenger load, road grade, and congestion level on real-world emissions and fuel consumption of urban Euro VI CNG and Euro V diesel buses. As the road grade and congestion level increased, both buses' fuel consumption and CO_2 emissions increased by 6–55%. Gallus et al. [15] studied the impact of driving style and road grade on gaseous exhaust emissions of Euro V and Euro VI diesel vehicles. CO_2 and NO_x emissions, measured with PEMS, showed a linear increase with road grade. Chen et al. [16] investigated the impact of speed and acceleration on emissions of heavy-duty (HD) vehicles in Shanghai. They found that congestion conditions with low speed and frequent deceleration and acceleration increased THC and CO emissions. Ozener & Ozkan [17] reported that the acceleration effect on both fuel consumption and emission values was significant. They concluded that the real-driving emission data could be effectively used in developing cleaner engine calibrations and more economical operations.

In addition, gaseous emissions are strongly affected by starting conditions. The cold-start emissions challenge has been highlighted, e.g., in [18,19]. During the first minutes of operation, emissions are high because the after-treatment equipment has not reached the appropriate temperature required to efficiently remove gaseous pollutants. Faria et al. [20] also showed a substantial increase in energy consumption for cold-start, leading to increased CO_2 emissions during the cold-start period. The problem of cold-starts is

considered more pronounced at low ambient temperatures, as lower ambient temperature increases the cold-start running duration [20,21].

One crucial topic rarely addressed in real-driving emissions (RDE) studies is the catalyst deactivation and deterioration over time. Indeed, the presence of catalyst poisons and other impurities in the feed, the fluctuating exhaust gas composition and flow rate in the converter, as well as high temperatures and temperature gradients, all increase the possibility of catalyst deactivation [22]. Therefore, to ensure a significant reduction of emission levels throughout the vehicle's useful life, EU regulation has adopted dedicated "emission durability" periods, i.e., the minimum mileage or time after which the engine is still expected to comply with applicable emission limits. For example, for category M3 buses, the required emission durability period is six years or 300,000 km, whichever comes first [23]. However, the useful life of urban buses is usually much longer; e.g., the Finnish bus fleet's average age is 12.5 years [24]. Therefore, emission levels after the emission durability period and closer to the service life of the vehicles need to be investigated.

This study focused on emissions from a six years old gas-powered city bus, supplementing emission data from aging bus fleets. PEMS measurements were performed in real-traffic conditions on a regular bus line in Vaasa in collaboration with the University of Vaasa and RISE Research Institutes of Sweden. In addition to methane emissions, gaseous emissions of NO_x, CO, and CO_2 were measured. Both cold-start and warm-engine emissions were recorded. We conducted two measurement campaigns, the first in March 2022 and the second in June 2022. In addition, the total carbon footprint of compressed biogas (CBG) is discussed in terms of its GHG reduction potential, defined as the percentage reduction in life cycle GHG emissions relative to its fossil counterpart natural gas and traditional diesel fuel.

2. Materials and Methods

2.1. Test Vehicle

Exhaust emission tests in real-driving conditions were carried out on a Scania Euro VI bus owned by the City of Vaasa and operated by Wasa Citybus. The CBG-fueled bus was equipped with a spark ignition engine with a displacement of 9.3 dm^3 and a power of 206 kW. The vehicle was equipped with exhaust gas recirculation (EGR) and a three-way catalytic converter. Table 1 presents the characteristics of the test vehicle and Table 2 summarizes the engine technical specifications.

Table 1. Vehicle technical specifications.

Parameter	Value
Model name	Scania Citywide LE
Model year	2016
Gross vehicle weight (kg)	19,100
Curb weight (kg)	12,960
Max passenger number	75
Axle configuration	4 × 2
Gearbox	6-speed automatic transmission
Accumulated mileage (km)	375,000 (Test 1), 400,000 (Test 2)
After-treatment system	TWC
Other systems	EGR
Exhaust emission norm	Euro VI-C

Table 2. Engine technical specifications.

Parameter	Value
Model	Scania OC09 101
Engine type	Spark ignition engine
Fuel	CNG/CBG

Table 2. *Cont.*

Parameter	Value
Number of cylinders	5
Compression ratio	12.6:1
Total displacement (L)	9.3
Maximum power (kW@rpm)	206 kW@1900 rpm
Engine peak torque (Nm@rpm)	1350 Nm@1000–1400 rpm

2.2. Portable Emissions Measurement System

The real-driving gaseous emissions of CH_4, CO, CO_2, NO, and NO_2 from the tested city bus were measured and recorded using an on-board VARIOplus Industrial device manufactured by MRU Messgeräte für Rauchgase und Umweltschutz GmbH. VARIOplus measures CH_4, CO, and CO_2 concentrations using a non-dispersive infrared (NDIR) sensor, and NO_x concentrations are measured using electrochemical cells. Table 3 shows the technical characteristics of the measurement apparatus used in this work.

Table 3. Technical characteristics of VARIOplus Industrial.

Parameter	Measurement Method	Accuracy
CH_4	NDIR—Non-dispersive infrared, range 0–10,000 ppm	$\pm2\%$
CO	NDIR—Non-dispersive infrared, range 0–10%	$\pm0.03\%$ or * $\pm3\%$ reading
CO_2	NDIR—Non-dispersive infrared, range 0–30%	$\pm0.05\%$ or * $\pm3\%$ reading
NO	electrochemical, range 0–1000 ppm	±5 ppm or * 5% reading
NO_2	electrochemical, range 0–200 ppm	±5 ppm or * 5% reading
O_2	electrochemical, range 0–10%	±0.2 Vol-% abs.
Sampling	1 Hz	

* = whichever is larger.

The engine speed, torque, coolant temperature, air flow, lambda, and the vehicle speed were recorded from the vehicle engine control unit (ECU) via an on-board diagnostics (OBD) system using Scania Diagnosis & Programmer (SDP3) software version 2.50.3 (in Test 1) and version 2.52.1 (in Test 2), copyright Scania CV AB, Scania Suomi Oy, Vaasa, Finland. The vehicle's position in terms of latitude, longitude, and altitude, and the vehicle speed data were registered using an external global positioning system (GPS). A dedicated weather station was used to register the ambient temperature, pressure, and relative humidity. The real-world emission data obtained with PEMS and the GPS and the weather data were collected and stored with the DEWESoft data acquisition system. All data were recorded with a frequency of 1 Hz. Prior to the data processing, the SDP3 and DEWESoft data were synchronized based on the vehicle speed from the ECU and the GPS.

An external power unit supplied the electrical power to the PEMS system. Figure 1 depicts the system set-up.

2.3. Test Route

Emission tests were performed in real-driving conditions on an urban route in Vaasa, i.e., in normal traffic and with normal driving patterns and typical passenger loads. The selected test route was the same route the bus usually travels daily. The measurements started in the morning at the same time and the same driver from Wasa Citybus was used in both measurement campaigns. Figure 2 shows the driving circuit chosen for the tests. The length of one circuit was 25.5 km, and the same circuit was run three times. The total test duration was approx. 3 h. The route included both urban and rural driving. The speed profile of the driving circuit is presented in Figure 3. Table 4 shows the percentages and mean velocities for three different driving speed ranges. The passenger load varied between 5 and 30 percent during the tests.

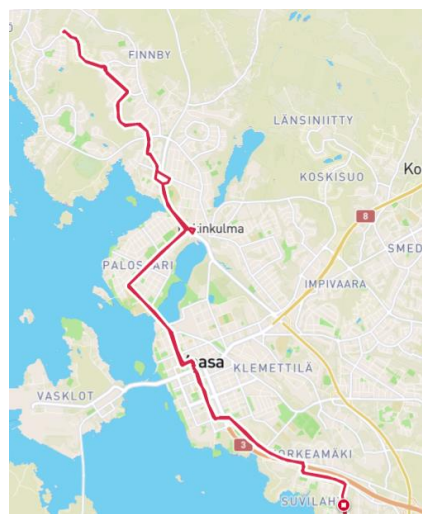**Figure 1.** Measurement system set-up.

Figure 2. Driving circuit.

The first measurement campaign was performed in March 2022, and the second in June 2022. In June, only warm engine measurements were recorded, while in March, both cold-start and hot-start emissions were investigated.

2.4. Fuel

The fuel used in the test was CBG from a commercial filling station. The methane content of the fuel was 97% by volume. The other main components of the fuel were CO_2 (2.2 vol.-%), nitrogen (0.5 vol.-%), and oxygen (0.3 vol.-%), so the energy content of the fuel was solely related to the methane concentration. The calculated lower heating value (LHV) of the gas was 46.4 MJ/kg.
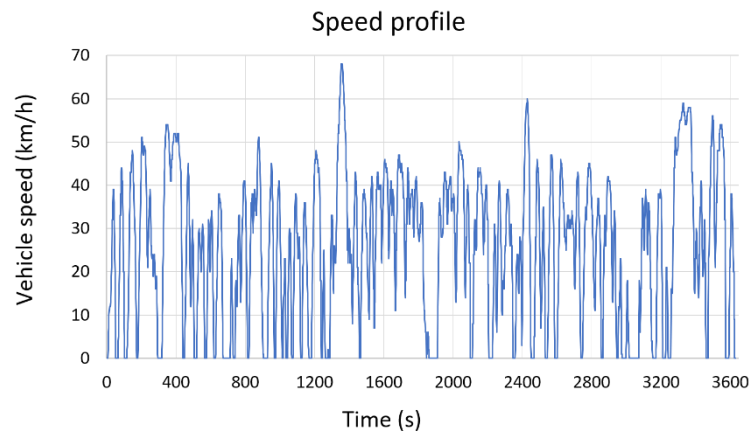
Speed profile

Figure 3. Speed profile of the driving circuit.

Table 4. Shares of driving speed ranges.

	Speed Range	Time (min)	%	Mean Velocity
Urban driving	0–30 km/h	102	56	12
Urban driving	30–50 km/h	65	36	38
Rural driving	50–75 km/h	16	9	57
Total		182		25

2.5. Calculation Procedure

2.5.1. Calculation of Fuel Mass Flow

The instantaneous fuel flow ($\dot{m}_{fuel}$) in kg/s was calculated based on the recorded instantaneous air flow ($\dot{m}_{air}$) and lambda (λ) values and the stoichiometric air-to-fuel ratio (AFR_{stoich}), according to Equation (1).

$$\dot{m}_{fuel} = \frac{\dot{m}_{air}}{AFR_{stoich} \times \lambda} \tag{1}$$

To determine AFR_{stoich}, the stoichiometric oxygen demand ($n_{O2,stoich}$) in moles per kg of fuel was calculated first, based on the chemical composition of the fuel (Equation (2)). In the equation, w_c, w_{H2} and w_{O2} are the fuel mass fractions of carbon, hydrogen and oxygen in the fuel.

$$n_{O2,\ stoich} = \frac{w_c}{0.012011} + \frac{1}{2} \times \frac{w_{H2}}{0.002016} - \frac{w_{O2}}{0.031999} \tag{2}$$

As air contains 20.95% of oxygen, the stoichiometric air demand ($n_{air,stoich}$) in moles per kg fuel could be determined by Equation (3):

$$n_{air,stoich} = \frac{n_{O2,stoich}}{0.2095} \tag{3}$$

Finally, the stoichiometric air demand in kg of air per kg of fuel was calculated by multiplying $n_{air,stoich}$ by the molar mass of air (M_{air}), see Equation (4):

$$AFR_{stoich} = n_{air,stoich} \times M_{air} \tag{4}$$

2.5.2. Calculation of Fuel Consumption

The total fuel mass (ΣFC_i) over the test cycle was calculated based on the instantaneous (second-by-second) fuel mass flows according to Equation (5).

$$\Sigma FC_i = \left(\frac{1}{2}\dot{m}_{fuel,0} + \dot{m}_{fuel,1} + \dot{m}_{fuel,2} + \ldots + \dot{m}_{fuel,n-1} + \frac{1}{2}\dot{m}_{fuel,n} \right) \tag{5}$$

2.5.3. Calculation of Exhaust Mass Flow

The instantaneous exhaust gas mass flow ($\dot{m}_{exh.,i}$) (wet basis) in kg/s was determined based on the recorded air flow and the calculated fuel flow values (Equation (6)):

$$\dot{m}_{exh.,i} = \dot{m}_{air,i} + \dot{m}_{fuel,i} \tag{6}$$

2.5.4. Emissions Dry–Wet Correction

The emission concentrations were measured on a dry basis. Dry concentration (c_{dry}) was converted to a wet basis with the dry–wet conversion factor (K_{d-w}):

$$c_{wet} = K_{d-w} \times c_{dry} \tag{7}$$

K_{d-w} was calculated according to the UN/ECE Regulation 49 [25], Equation (8):

$$K_{d-w} = \left(\frac{1}{1 + a \times 0.005 \times (c_{CO2} + c_{CO})} - k_{w1} \right) \times 1.008 \tag{8}$$

where a is the molar hydrogen to carbon ratio of the fuel, and

$$k_{w1} = \frac{1.608 \times H_a}{1000 + (1.608 \times H_a)} \tag{9}$$

where H_a is the intake air humidity in g water per kg dry air.

2.5.5. Calculation of Mass Emissions

Second-by-second mass flow of the pollutant ($\dot{m}_{gas}$) in g/s was calculated using Equation (10):

$$\dot{m}_{gas} = u_{gas} \times c_{gas} \times \dot{m}_{exh.} \tag{10}$$

where u_{gas} is the ratio between the density of pollutant and the density of exhaust gas, and c_{gas} is the instantaneous concentration of the pollutant in raw exhaust in ppm (wet basis). The instantaneous u values were calculated following the UN/ECE Regulation No 49 [25], according to Equations (11)–(14):

$$u_{gas,i} = \frac{\rho_{gas}}{(\rho_{exh.,i} \times 1000)} \tag{11}$$

$$\rho_{gas} = \frac{M_{gas}}{22.414} \tag{12}$$

where M_{gas} is the molar mass of the gas component in g/mol, ρ_{gas} is the density of the gas component in kg/m³, and $\rho_{exh.,i}$ the instantaneous density of the exhaust gas in kg/m³, derived from Equation (13):

$$\rho_{exh.,i} = \frac{1000 + H_a + 1000 \times \left(\frac{\dot{m}_{fuel,i}}{\dot{m}_{dry\ air,i}} \right)}{773.4 + 1.2434 \times H_a + k_{fw} \times 1000 \times \left(\frac{\dot{m}_{fuel,i}}{\dot{m}_{dry\ air,i}} \right)} \tag{13}$$

where k_{fw} is the fuel specific factor of wet exhaust, obtained from Equation (14):

$$k_{fw} = 0.055594 \times W_\alpha + 0.0080021 \times W_\Delta + 0.0070046 \times W_\varepsilon \tag{14}$$

where W_α is the hydrogen content (wt%) of the fuel, W_Δ the nitrogen content (wt%), and W_ε the oxygen content (wt%) of the fuel.

The mass of gaseous emissions (m_{gas}) in grams per test cycle was calculated using Equation (15).

$$m_{gas} = \sum_{i=1}^{i=n} u_{gas,i} \times c_{gas,i} \times \dot{m}_{exh.,i} \times \frac{1}{f} \tag{15}$$

where f is the data sampling rate in Hz.

The final results are expressed in g/kWh and in g/km, i.e., the total mass of each pollutant over the test cycle was divided by the engine cycle work or by the distance covered in km.

2.5.6. Calculation of Cycle Work

The engine work (W_i) in kWh over the test cycle was calculated based on the instantaneous (second-by-second) engine power values (P_e), according to Equation (16):

$$W_i = \frac{\left(\frac{1}{2}P_{e,0} + P_{e,1} + P_{e,2} + \ldots + P_{e,n-2} + P_{e,n-1} + \frac{1}{2}P_{e,n}\right)}{3600} \tag{16}$$

2.5.7. Calculation of Effective Power of the Engine

The instantaneous engine power in kW was calculated by using each pair of recorded engine speed and torque values (Equation (17)):

$$P_e = \frac{2 \times \pi \times N \times \tau}{60 \times 1000} \tag{17}$$

where N is the engine speed in rpm and τ is the engine torque in Nm.

3. Results and Discussion

3.1. Ambient Conditions

Table 5 summarizes the average ambient conditions during the tests.

Table 5. Ambient conditions during the tests.

Ambient Condition	Test 1	Test 2
	March 2022	**June 2022**
Temperature (°C)	−5 °C	+18 °C
Pressure (kPa)	102.5	100.5
Humidity (%)	65.5	54.7

3.2. Gaseous Emissions

In the current legislation, the regulatory in-service conformity (ISC) emission test applies the 20% power threshold as a boundary condition for Euro VI-C bus engines. However, Mendoza Villafuerte et al. [26] showed that a large fraction of urban operation is not considered if the current power threshold boundary for post-processing the PEMS data is applied, and up to 80% of the data may be excluded from the emission analysis. They also showed that cold-start emissions, which are currently also excluded from the analysis, could account for a significant proportion of total emissions. To give a more accurate depiction of real-driving emissions, no power threshold boundaries were applied in this study. In addition, in Test 1, both cold-start and hot-start emissions were recorded. In Test 2, unfortunately, only hot-start emissions were successfully recorded.

3.2.1. Hot-Start Emissions

A test was considered a hot-start once the coolant temperature had reached 70 °C for the first time or stabilized within ±2 °C over a period of 5 min, whichever came first [27]. Specific emissions were calculated in both g/kWh and g/km, and the results are presented separately for the total trip and for urban and rural sections of the circuit (Figure 4). Although the tests performed did not fully reflect the ISC tests in the type-approval procedure regarding boundary conditions and route requirements, the Euro VI standard limits (ISC limit) are also presented for comparative purposes.
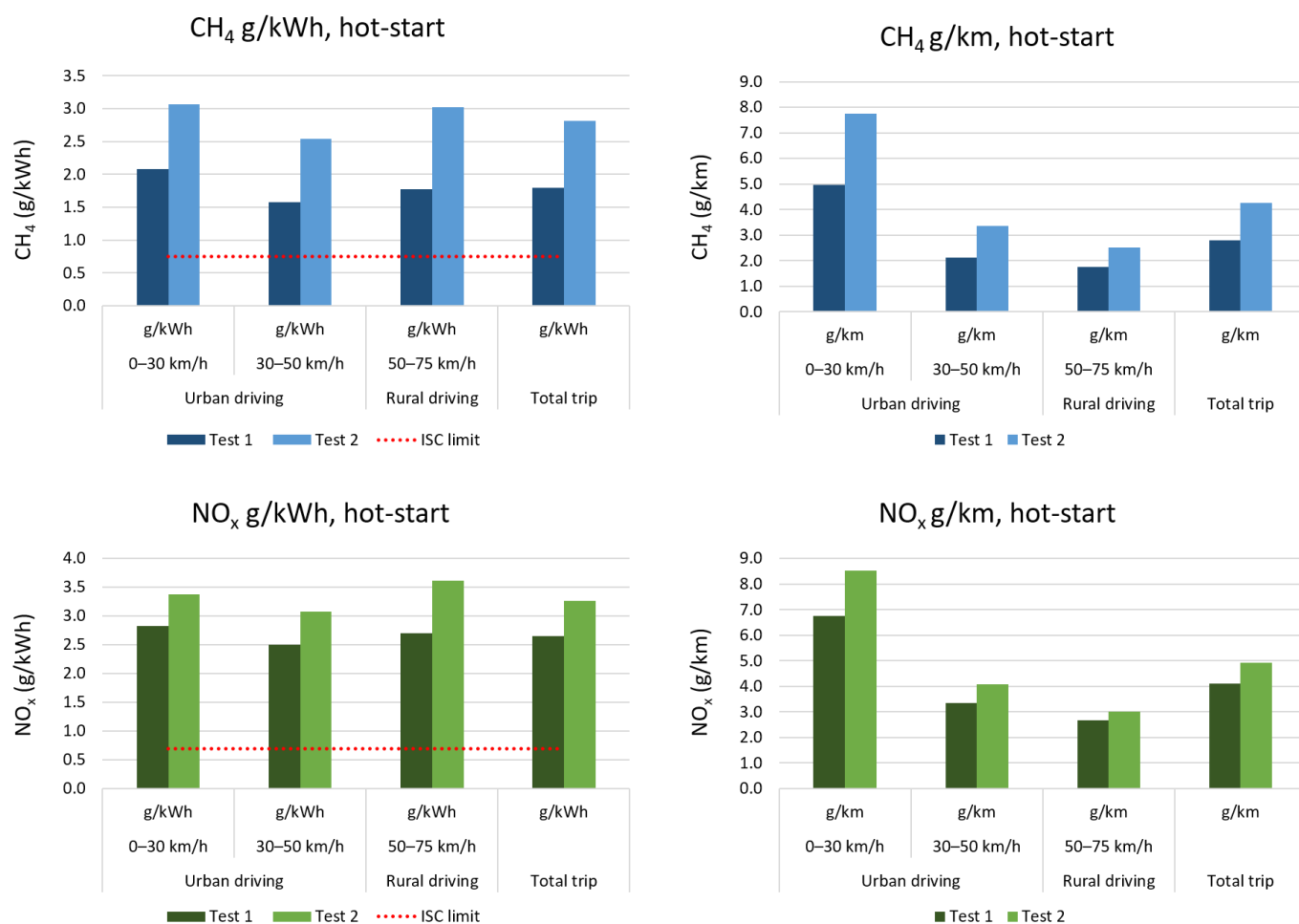
Figure 4. Specific CH_4 and NO_x emissions in g/kWh and g/km in hot-start tests.

CO emission values were low and well below the ISC limit of 6 g/kWh in both tests, indicating efficient oxidation of CO in the catalyst. In contrast, relatively high values were observed for CH_4 and NO_x, indicating impaired CH_4 oxidation and NO_x reduction in the catalyst after its service life of 375,000 km (Test 1). After 400,000 km (Test 2), the catalyst efficiency had further deteriorated. Here, it should be noted that according to EU Regulation EC 595/2009 [23], the minimum mileage or time after which the engine is still expected to comply with applicable emission limits for category M3 buses, is 300,000 km or six years, whichever comes first. Hence, the required "emission durability" period had already been exceeded in our case. Nevertheless, the bus has passed the regular technical inspections valid in Finland, including CO_2 and HC measurements.

The primary reason for relatively high CH_4 and NO_x emissions after the TWC was assumed to be the low CH_4 reactivity due to a partial deactivation of the catalyst. In addition to the low CH_4 oxidation rate, low CH_4 reactivity also means that methane-based reducing agents for NO_x reduction do not work, leading to substantial NO_x breakthrough from the catalyst, also concluded by Van den Brink & McDonald [28].

One of the most important reasons for the deactivation of the TWC in automotive applications is chemical deactivation [29], mainly caused by lubricating oil additives and other impurities in the exhaust gases. For example, Winkler et al. [30] observed a significant increase in hydrocarbon emissions during CNG operation over a relatively short TWC lifetime of 35,000 km. Contaminants originating from the lubricating oil, such as calcium, phosphorus, and magnesium, detected on the catalyst's surface, appeared to affect especially CH_4 oxidation. In addition to lubricating oil, another source of catalyst poisons is the impurities in the fuel. The CBG used in this study contained small traces of commonly

encountered catalyst poison sulfur (<2.3 mg/Nm^3) and siloxanes (0.7 mg/Nm^3). Although the amounts of these compounds were very low, they could have had a deactivating effect on the emissions control system.

Furthermore, the light-off of a TWC in gas-fueled engine exhaust typically occurs at higher temperatures compared to gasoline engines [31]. Indeed, methane is the most difficult hydrocarbon to oxidize due to its high stability [8]. A typical light-off temperature for methane is 400 °C [8], but in a deactivated catalyst, significantly higher temperatures, up to 500–600 °C [32], may be required to break the strong C–H bonds in methane. At low loads (Figure 5), common in a city bus's driving profile, the exhaust gas temperature was too low to allow the deactivated catalyst to work effectively.
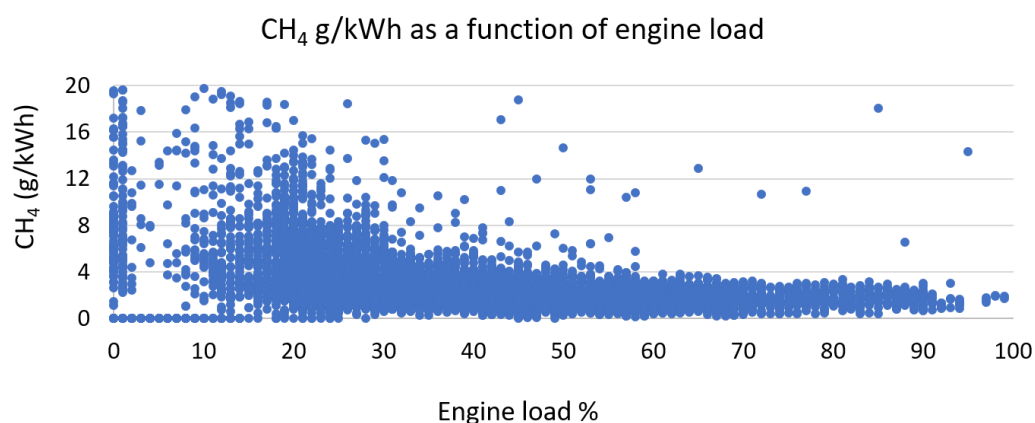
CH$_4$ g/kWh as a function of engine load

Figure 5. Specific CH$_4$ emissions as a function of engine load%.

Thus, restoring the catalytic activity of a deactivated TWC is a critical consideration. In some cases, depending on the adsorbed poison, the activity of the poisoned catalyst can be at least partially restored by regeneration [22]. For example, SO$_2$ can be removed from the catalyst under elevated temperatures and anoxic or very rich conditions, as shown by Auvinen et al. [32]. Careful control of the exhaust gas composition during regeneration could provide significant benefits in terms of CH$_4$ emissions. However, under real-driving conditions, the rapidly and dramatically varying exhaust gas temperature and composition between oxidizing and reducing environment make the on-board regeneration difficult to control.

Another possible deactivation mechanism for the TWC is thermal degradation. Three-way catalysts are known to lose their activity when exposed to high temperature (>800 °C) oxidizing environments, typically occurring during fuel shut-off phases [33]. Switching off the fuel flow, e.g., during engine braking, is a strategy of the automotive industry to improve fuel economy. Thermal degradation is critical to the catalyst's performance since these changes are typically irreversible.

In addition to the partial deactivation of the catalyst, another probable reason for the relatively high emissions was the fluctuating lambda value. Indeed, close control of the exhaust gas composition is essential for high emission conversion as the composition of the gas entering the TWC significantly affects its catalytic efficiency [34]. For simultaneous conversion of HC, CO, and NO$_x$ species in the TWC, the engine must be operated within a very narrow AFR window—near stoichiometric conditions—due to a rapid drop in NO$_x$ conversion efficiency on the lean side and a non-complete conversion of hydrocarbons both in lean and rich stoichiometry [10]. For example, Lou et al. [34] detected the highest TWC conversion efficiency when AFR was controlled between 0.995 and 1. The narrow AFR range over which significant conversion of natural gas exhaust emissions is possible presents a challenging control problem. As seen in Figure 6, lambda was outside the optimal range for a significant part of the time in our experiments.
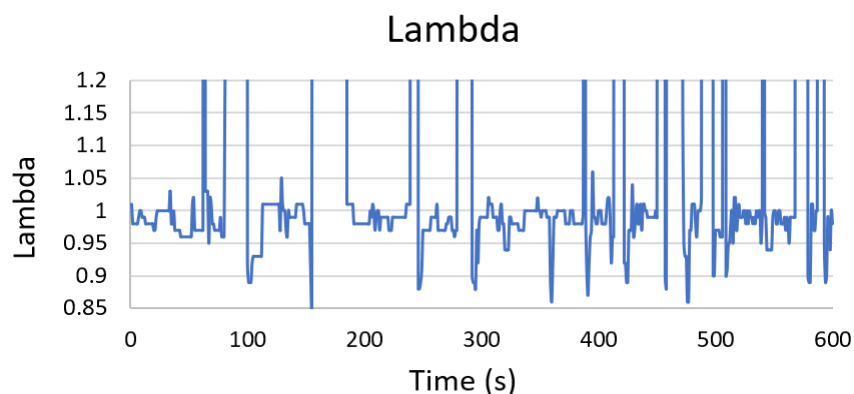
Figure 6. Fluctuating lambda values under real-driving conditions.

In sum, deterioration of the exhaust after-treatment systems over time should be monitored as they are exposed to different aging processes resulting in elevated real-world emissions. Our results indicate a catalyst replacement need after 375,000 km of service life. In addition, a precise lambda control is absolutely necessary to ensure high conversion rates throughout the vehicle's lifetime.

3.2.2. Cold-Start Emissions

Cold-start emissions were recorded from the moment the coolant temperature had reached 30 °C for the first time and continued until the coolant temperature was stabilized within ±2°C over 5 min [27]. In Test 1 (at −5 °C), the cold-start period lasted 14.5 min. The combined cold- and hot-start emissions were calculated according to EU Regulation 1718 [35]: the vehicle was driven over a cold-test cycle followed by nine hot-test cycles, identical to the cold one in a way that the work developed by the engine was the same as the one achieved in the cold cycle.

Figure 7 illustrates CH_4 and NO_x emissions during cold-start versus hot-start. During the cold-start, CH_4 emissions were 2.3 times higher and NO_x emissions 1.4 times higher than those during the hot-start. This highlights the temperature sensitivity of catalytic emission control systems, which is also evidenced in Figure 8.
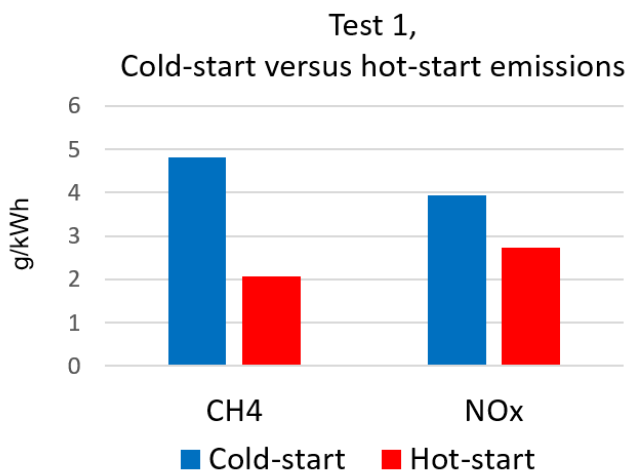

Figure 7. Cold-start versus hot-start emissions.

Over the combined cold- and hot-start cycles, CH_4 emissions increased by 30%, NO_x by 13%, and CO by 33% compared to hot-start-only measurements.

The cold-start emissions challenge is more pronounced at low ambient temperatures because it then takes longer for the TWC to reach effective operating temperature, leading to a prolonged period of high emission rates [18,20,21].
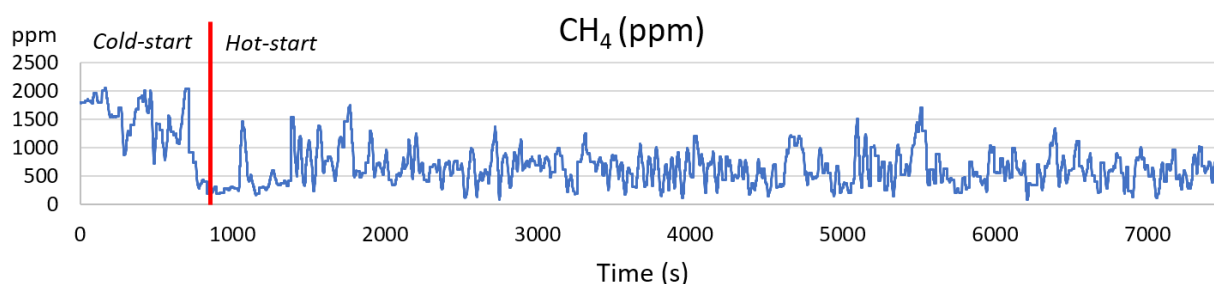
Figure 8. CH$_4$ emissions during combined cold- and hot-start test.

3.3. Well-to-Wheels Analysis

In the transport sector, well-to-wheels (WTW) analysis is a commonly used method for assessing the carbon intensity of a fuel. Carbon intensity refers to the amount of greenhouse gases—including CO_2, nitrous oxide, and methane—released during the production and consumption of a transportation fuel, measured in grams of carbon dioxide equivalent per megajoule of energy (g CO_2-eq./MJ).

3.3.1. Fuel Consumption

The total fuel consumption in the hot-start test at $-5\,^\circ$C was 21.9 MJ/km (6.1 kWh/km), corresponding to 0.306 kg/kWh and 47.1 kg/100 km. In June, at $+18\,^\circ$C, the vehicle showed better fuel economy with fuel consumption of 19.8 MJ/km (5.5 kWh/km), corresponding to 0.283 kg/kWh and 42.7 kg/100 km (Figure 9).
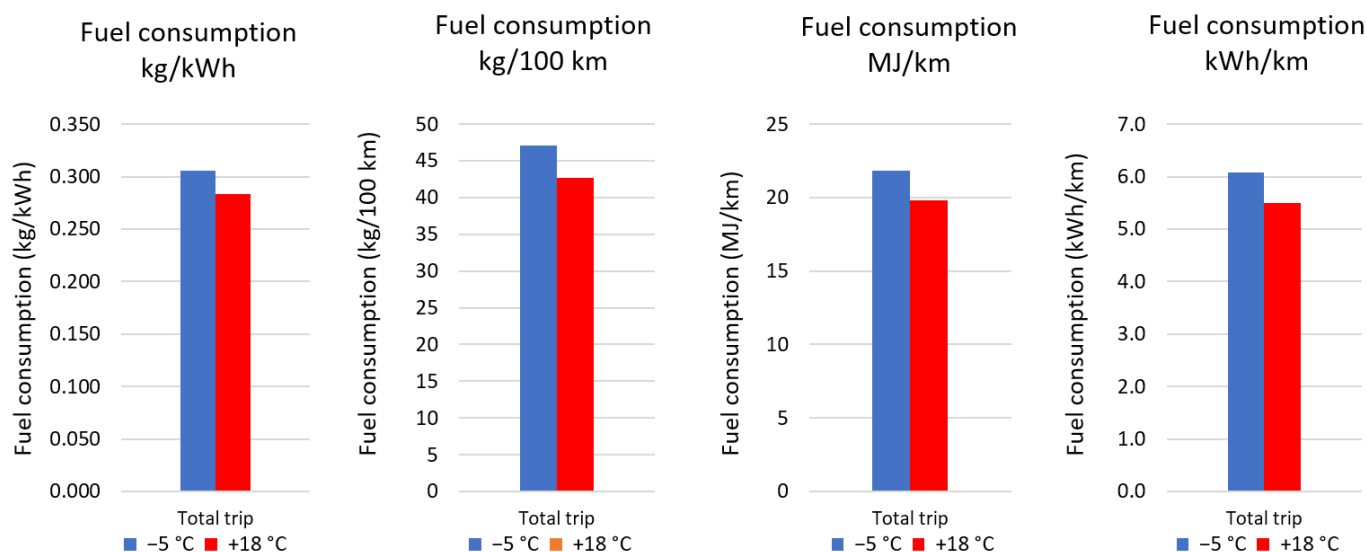

Figure 9. Fuel consumption in hot-start tests at $-5\,^\circ$C and $+18\,^\circ$C.

3.3.2. Biogas Production Process

The life cycle steps for CBG investigated in this study are feedstock collection and transportation, biogas production, biogas processing to biomethane, biomethane compression, and finally, combustion in an engine. The CBG was produced at Stormossen waste treatment plant near Vaasa. The anaerobic digestion process at Stormossen is divided into two separate process lines. Biogas reactor 1 is fed with wastewater sludge, and the raw material used in biogas reactor 2 is municipal biowaste, supplied within a radius of 40 km [36].

In 2020, raw biogas production at Stormossen was 2.7 million Nm^3, of which 52% was upgraded into biomethane, 32% was used for heat and electricity production, and the rest was flared [37]. The methane content of the raw biogas was 62%.

The biogas upgrading is executed by an amine scrubber. The main advantages of chemical absorption with amine solvents are a high methane recovery rate in the upgraded biogas and a low methane slip of <0.1% [38]. In addition, amine solvents are effective at near atmospheric pressure and thus consume a low quantity of electric energy [39]. On the other hand, chemical scrubbing liquids require substantial thermal energy during regeneration, which must be supplied as process heat [39]. After the refining stage, biogas contains 97–98% methane. Finally, the processed biomethane is piped to a gas filling station near the biogas plant. At the refueling station, the gas is pressurized to 300 bar and stored in gas cylinders.

Although the combustion of waste-based biomethane is considered carbon-neutral in Finland's national GHG inventories (CO_2 emissions from biogas combustion are reported as zero), the use of biomethane may still have climate impact from the above-mentioned earlier stages of the fuel chain. For CBG production, the major contributors of GHG emissions are energy consumption and fugitive losses of methane during digestion and upgrading processes [40]. In addition, some GHG emissions form during the collection of wastes and residues.

3.3.3. GHG Inventory

In this study, the calculation of GHG emissions begins with feedstock collection and transportation. GHG emissions from these steps are based on the following assumptions. Transportation distance 40 km and diesel B7 fuel consumption 20 l/100 km. The lower calorific value of diesel B7 fuel is 43 MJ/kg. The biocomponent of diesel fuel was assumed to be hydrotreated vegetable oil made from waste materials, so the calculated well-to-tank emission factor for diesel B7 was 14.7 g CO_2-eq./MJ fuel, based on the JRC [41] data. Tank-to-wheels CO_2 emission factor for diesel B7 was set at 68.4 g CO_2-eq./MJ fuel [42]. The heat and electricity needs of biogas production and upgrading processes are covered internally by the plant's own CHP biogas engine and were, therefore, ignored in the GHG inventory. Methane emissions were calculated assuming a methane loss of 1% during anaerobic digestion [43] and 0.1% during the upgrading process [39]. Methane emissions are converted to CO_2-equivalents using a 100-year time horizon global warming potential (GWP) factor of 28 [7]. The energy demand for biomethane compression to 300 bar is 0.25 kWh/m^3 (NTP) [44], and the electric energy for compression is taken from the public grid. The CO_2 emission factor for electricity generation in Finland in 2020 was 68.6 g CO_2-eq./kWh [45]. Table 6 summarizes the main assumptions and input data used in the calculation.

Table 6. CBG well-to-tank GHG emissions.

Parameter	Value	Unit	g CH_4/$MJ_{bio-CH4}$	g CO_2-Equivalent /$MJ_{bio-CH4}$	Source
Feedstock collection and transportation					
Diesel trucks, diesel fuel biocomponent 7%	40	km		1.95	[41,42]
Biogas production and refining					
Total biogas production	2,716,000	Nm^3			[37]
52% of raw gas for upgrading	1,412,320	Nm^3			[37]
Methane content (62%)	875,638	Nm^3			[37]
Total biomethane production	31,522,982	MJ			
Heat demand *					
- Anaerobic digestion	0.19	kWh/$Nm^3_{raw\ gas}$			[43]
- Upgrading	0.110	kWh/$kWh_{bio-CH4}$			
Electricity demand *					
- Anaerobic digestion	0.14	kWh/$Nm^3_{raw\ gas}$			[43]
- Upgrading	0.0136	kWh/$kWh_{bio-CH4}$			
Methane losses					
- Anaerobic digestion, 1%	6368	kg	0.202	5.66	[43]
- Upgrading, 0.1%	630	kg	0.020	0.56	[39]

Table 6. *Cont.*

Parameter	Value	Unit	g CH$_4$/MJ$_{bio-CH4}$	g CO$_2$-Equivalent /MJ$_{bio-CH4}$	Source
Compression Electricity demand	0.25	kWh/m^3 (NTP)		0.48	[44,45]
CBG well-to-tank GHG emissions				8.65	

* Covered internally by the plant's own CHP biogas engine.

After the anaerobic digestion, the digestate is dewatered and composted to be used as a soil improvement product or as landscaping soil. The digestate treatment is not included in the above table. Any fertilizer or sludge credits are also not considered in GHG calculations.

The GHG benefits associated with transition from fossil-based natural gas or diesel to biomethane were calculated by comparing well-to-wheels CO$_2$-Equivalent emissions, shown in Table 7. Well-to-tank GHG emission factors for compressed natural gas and diesel fuel were taken from the JRC report [41]. Tank-to-wheel GHG emissions for gas buses are based on the CO$_2$ and CH$_4$ emission results recorded in this study, but CO$_2$ emissions are considered only for fossil CNG. Tank-to-wheels CO$_2$ emission factor for diesel buses was taken from [42]. The average fuel consumption from Test 1 and 2 in this study was 20.8 MJ/km, and this value is applied to both CBG and CNG bus. It is well known that compression-ignition diesel engines have higher thermal efficiency compared to spark ignition gas engines. Therefore, the fuel consumption of a diesel bus was set at 80% of that of a gas bus, based on the VTT's (Technical Research Centre of Finland) comprehensive report on city bus emissions measurements [46].

Table 7. Well-to-wheels CO$_2$ Equivalent emissions for CBG, CNG, and diesel B7.

	CBG	CNG	Diesel B7
GHG emissions Well-to-tank (g/MJ$_{fuel}$)	8.65	13.0	14.7
Tank-to-wheels			
• CO$_2$ (g/MJ$_{fuel}$)		46.6	68.4
• CH$_4$ (g/MJ$_{fuel}$)	0.1708	0.1708	
Total GHG (g CO$_2$-eq./MJ$_{fuel}$)	13.4	64.4	83.1
Fuel consumption (MJ/km)	20.8	20.8	16.7
Specific GHG (g CO$_2$-eq./km)	**279**	**1342**	**1385**

Figure 10 shows the percentage changes in life cycle GHGs for the studied fuels. Shifting from conventional diesel to fossil natural gas does not show meaningful GHG benefits, bearing in mind the higher thermal efficiency of compression-ignition engines compared to spark-ignition gas engines. However, for biomethane, the situation is very different; 80% GHG emission benefit is achieved by switching from diesel to biomethane. With more precise methane emission control, GHG emission savings would advance towards 90%.
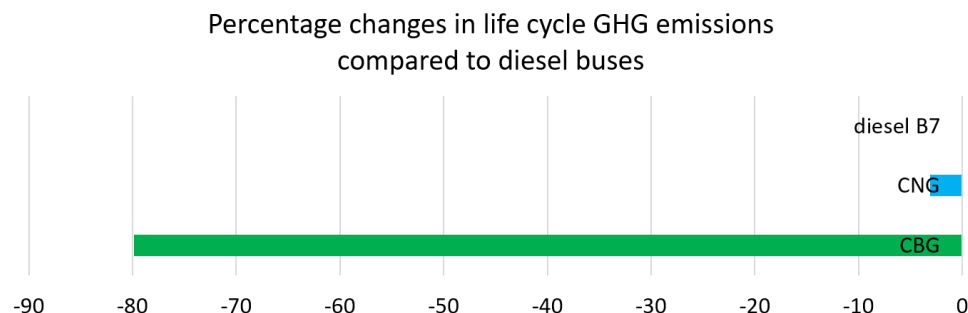

Figure 10. Percentage changes in life cycle GHGs.

This gives a strong environmental argument for biogas use. Increasing biogas use would be a quick and cost-effective way to reduce GHG emissions from urban traffic. Unfortunately, the potential of renewable gas is not acknowledged in the current EU emission standards, which only focus on tank-to-wheels emissions. Changing the measurement method to life cycle-based WTW instead of tailpipe measurement would enable a proper assessment of GHG emissions of future vehicle technology and fuel combinations. However, the results of this study can be utilized in designing strategies for transitioning to sustainable urban transport systems.

4. Conclusions

Transition to low-emission transportation and cleaner cities requires a broad introduction of low- and zero-carbon alternatives to conventional petrol- and diesel-powered vehicles. This paper presents the results of real-driving emission measurements from a Euro VI biogas-powered city bus equipped with a TWC. In addition, the lifetime carbon intensity of CBG was investigated and compared to its fossil counterpart CNG and traditional diesel fuel. The main findings were, first, for the bus:

- The rapid changes in exhaust gas temperature and composition under transient driving conditions seemed to be a critical challenge to an efficient operation of the TWC.
- Unimpressive CH_4 oxidation and NO_x reduction were observed in the catalyst after its service life of 375,000 km–400,000 km. In contrast, CO emissions were low, indicating efficient oxidation of CO in the catalyst.
- The primary reason for deficient CH_4 and NO_x conversion over the TWC was assumed to be the low CH_4 reactivity due to a partial deactivation of the catalyst. At low loads, common in a city bus's driving profile, the exhaust gas temperature was too low to allow efficient CH_4 oxidation. In addition to the low CH_4 oxidation rate, low CH_4 reactivity also means that methane-based reducing agents for NO_x reduction do not work, leading to substantial NO_x breakthrough from the catalyst.
- In addition, during the cold-start, CH_4 emissions were 2.3 times and NO_x emissions 1.4 times as high as those during the hot-start, highlighting the temperature sensitivity of catalytic emission control systems.
- Based on the above, deterioration of the exhaust after-treatment systems over time should be monitored as they are exposed to different aging processes resulting in elevated real-world emissions.
- Another critical issue was the fluctuating air-to-fuel ratio. Lambda was outside the optimal range for a significant part of the time, likely reducing the TWC efficiency. This highlights the need for precise lambda control to ensure high conversion rates throughout the vehicle's lifetime.

    Additionally,

- The WTW analysis showed an 80% GHG emission benefit by switching from diesel to biomethane, giving a strong environmental argument for biogas use. With more precise methane emission control, GHG emission savings would advance towards 90%.

The presented real-driving emission results are of great importance in supplementing the emission data for aging gas-powered HD vehicles, filling the gap of data on emissions closer to the service life of the vehicles. After all, the average age of bus fleets in Finland, for example, is over 12 years. The results of this study can also be utilized in scheduling catalyst maintenance or replacement activities.

In the future, it would be worthwhile to repeat the weather-related comparison with a completely new bus or with a new catalyst on an old bus.

Data Availability Statement: Not applicable.

Conflicts of Interest: The authors declare no conflict of interest.

Abbreviations

The following abbreviations are used in this manuscript:

AFR	air-to-fuel ratio
CAN	controller area network
CH_4	methane
CO	carbon monoxide
CO_2	carbon dioxide
CBG	compressed biogas
CNG	compressed natural gas
ECU	engine control unit
EGR	exhaust gas recirculation
GPS	global positioning system
HC	hydrocarbon
HD	heavy-duty
ISC	in-service conformity
NDIR	non-dispersive infrared
NO	nitrogen monoxide
NO_2	nitrogen dioxide
NO_x	nitrogen oxides
OBD	on-board diagnostics
PEMS	portable emissions measurement system
PM	particulate matter
RDE	real-driving emissions
THC	total hydrocarbons
TWC	three-way catalyst
WTW	well-to-wheels

References

1. Communication from the Commission to the European Parliament, the Council, the European Economic and Social Committee and the Committee of the Regions. Stepping up Europe's 2030 Climate Ambition. Investing in a Climate-Neutral Future for the Benefit of Our People. EU COM/2020/562 Final. Available online: https://eur-lex.europa.eu/legal-content/EN/TXT/?uri=CELEX%3A52020DC0562 (accessed on 14 May 2022).
2. Finnish Government; Marin's Government; Government Programme. Strategic Themes. 3.1 Carbon Neutral Finland that Protects Biodiversity. Available online: https://valtioneuvosto.fi/en/marin/government-programme/carbon-neutral-finland-that-protects-biodiversity (accessed on 2 May 2022).
3. Liikennefakta. Liikenteen Kasvihuonekaasupäästöt ja Energiankulutus. Finnish Transport and Communications Agency Traficom. Available online: https://liikennefakta.fi/fi/ymparisto/liikenteen-kasvihuonekaasupaastot-ja-energiankulutus (accessed on 2 May 2022).
4. Franco, V.; Kousoulidou, M.; Muntean, M.; Ntziachristos, L.; Hausberger, S.; Dilara, P. Road vehicle emission factors development: A review. *Atmos. Environ.* **2013**, *70*, 84–97. [CrossRef]
5. Biernat, K.; Samson-Bręk, I.; Chłopek, Z.; Owczuk, M.; Matuszewska, A. Assessment of the Environmental Impact of Using Methane Fuels to Supply Internal Combustion Engines. *Energies* **2021**, *14*, 3356. [CrossRef]
6. Biogenic Carbon Dioxide. The Finnish Innovation Fund Sitra. Available online: https://www.sitra.fi/en/dictionary/biogenic-carbon-dioxide/ (accessed on 2 May 2022).

7. Myhre, G.; Shindell, D.; Bréon, F.-M.; Collins, W.; Fuglestvedt, J.; Huang, J.; Koch, D.; Lamarque, J.-F.; Lee, D.; Mendoza, B.; et al. Anthropogenic and Natural Radiative Forcing. In *Climate Change 2013: The Physical Science Basis*; Contribution of Working Group I to the Fifth Assessment Report of the Intergovernmental Panel on Climate Change; Stocker, T.F., Qin, D., Plattner, G.-K., Tignor, M., Allen, S.K., Boschung, J., Nauels, A., Xia, Y., Bex, V., Midgley, P.M., Eds.; Cambridge University Press: Cambridge, UK; New York, NY, USA, 2013; pp. 659–740. Available online: https://www.ipcc.ch/site/assets/uploads/2018/02/WG1AR5_Chapter08_FINAL.pdf (accessed on 16 May 2022).
8. Stoian, M.; Rogé, V.; Lazar, L.; Maurer, T.; Védrine, J.C.; Marcu, I.C.; Fechete, I. Total Oxidation of Methane on Oxide and Mixed Oxide Ceria-Containing Catalysts. *Catalysts* **2021**, *11*, 427. [CrossRef]
9. Pan, D.; Tao, L.; Sun, K.; Golston, L.M.; Miller, D.J.; Zhu, T.; Qin, Y.; Zhang, Y.; Mauzerall, D.L.; Zondlo, M.A. Methane emissions from natural gas vehicles in China. *Nat. Commun.* **2020**, *11*, 4588. [CrossRef]
10. Di Maio, D.; Beatrice, C.; Fraioli, V.; Napolitano, P.; Golini, S.; Rutigliano, F.G. Modeling of Three-Way Catalyst Dynamics for a Compressed Natural Gas Engine during Lean–Rich Transitions. *Appl. Sci.* **2019**, *9*, 4610. [CrossRef]
11. Rodman Oprešnik, S.; Seljak, T.; Vihar, R.; Gerbec, M.; Katrašnik, T. Real-World Fuel Consumption, Fuel Cost and Exhaust Emissions of Different Bus Powertrain Technologies. *Energies* **2018**, *11*, 2160. [CrossRef]
12. Gis, M.; Pielecha, J.; Gis, W. Exhaust emissions of buses LNG and Diesel in RDE tests. *Open Eng.* **2021**, *11*, 356–364. [CrossRef]
13. Lv, L.; Ge, Y.; Ji, Z.; Tan, J.; Wang, X.; Hao, L.; Wang, Z.; Zhang, M.; Wang, C.; Liu, H. Regulated emission characteristics of in-use LNG and diesel semi-trailer towing vehicles under real driving conditions using PEMS. *J. Environ. Sci.* **2020**, *88*, 155–164. [CrossRef]
14. Rosero, F.; Fonseca, N.; López, J.M.; Casanova, J. Effects of passenger load, road grade, and congestion level on real-world fuel consumption and emissions from compressed natural gas and diesel urban buses. *Appl. Energy* **2021**, *282*, 116195. [CrossRef]
15. Gallus, J.; Kirchner, U.; Vogt, R.; Benter, T. Impact of driving style and road grade on gaseous exhaust emissions of passenger vehicles measured by a Portable Emission Measurement System (PEMS). *Transp. Res. D Transp. Environ.* **2017**, *52*, 215–226. [CrossRef]
16. Chen, C.; Huang, C.; Jing, Q.; Wang, H.; Pan, H.; Li, L.; Zhao, J.; Dai, Y.; Huang, H.; Schipper, L.; et al. On-road emission characteristics of heavy-duty diesel vehicles in Shanghai. *Atmos. Environ.* **2007**, *41*, 5334–5344. [CrossRef]
17. Ozener, O.; Ozkan, M. Assessment of real driving emissions of a bus operating on a dedicated route. *Therm. Sci.* **2020**, *24*, 66–73. [CrossRef]
18. Giechaskiel, B.; Valverde, V.; Kontses, A.; Suarez-Bertoa, R.; Selleri, T.; Melas, A.; Otura, M.; Ferrarese, C.; Martini, G.; Balazs, A.; et al. Effect of Extreme Temperatures and Driving Conditions on Gaseous Pollutants of a Euro 6d-Temp Gasoline Vehicle. *Atmosphere* **2021**, *12*, 1011. [CrossRef]
19. Reiter, M.S.; Kockelman, K.M. The problem of cold starts: A closer look at mobile source emissions levels. *Transp. Res. D Transp. Environ.* **2016**, *43*, 123–132. [CrossRef]
20. Faria, M.V.; Varella, R.A.; Duarte, G.O.; Farias, T.L.; Baptista, P.C. Engine Cold Start Analysis Using Naturalistic Driving Data: City Level Impacts on Local Pollutants Emissions and Energy Consumption. *Sci. Total Environ.* **2018**, *630*, 544–559. [CrossRef]
21. Yusuf, A.A.; Inambao, F.L. Effect of cold start emissions from gasoline-fueled engines of light-duty vehicles at low and high ambient temperatures: Recent trends. *Case Stud. Therm. Eng.* **2019**, *14*, 100417. [CrossRef]
22. Lassi, U. Deactivation Correlations of Pd/Rh Three-way Catalysts Designed for Euro IV Emission Limits. Effect of Ageing Atmosphere, Temperature and Time. Academic Dissertation, University of Oulu, Department of Process and Environmental Engineering, Oulu, Finland, 2003. Available online: http://jultika.oulu.fi/files/isbn9514269543.pdf (accessed on 8 June 2022).
23. Regulation No 595/2009 of the European Parliament and of the Council of 18 June 2009 on Type-Approval of Motor Vehicles and Engines with Respect to Emissions from Heavy Duty Vehicles (Euro VI) and Amending Regulation (EC) No 715/2007 and Directive 2007/46/EC and Repealing Directives 80/1269/EEC, 2005/55/EC and 2005/78/EC. EC 595/2009. Available online: https://eur-lex.europa.eu/legal-content/EN/TXT/PDF/?uri=CELEX:02009R0595-20200901&from=EN (accessed on 14 May 2022).
24. ACEA. Facts and Figures. Average age of the EU Vehicle Fleet, by Country. Available online: https://www.acea.auto/figure/average-age-of-eu-vehicle-fleet-by-country/ (accessed on 20 June 2022).
25. Regulation No 49 of the Economic Commission for Europe of the United Nations (UN/ECE)—Uniform Provisions Concerning the Measures to be Taken against the Emission of Gaseous and Particulate Pollutants from Compression-Ignition Engines and Positive Ignition Engines for Use in Vehicles. UN/ECE 49/2013. Available online: https://eur-lex.europa.eu/legal-content/EN/TXT/PDF/?uri=CELEX:42013X0624(01)&from=EN (accessed on 12 May 2022).
26. Mendoza Villafuerte, P.; Suarez Bertoa, R.; Giechaskiel, B.; Riccobono, F.; Bulgheroni, C.; Astorga, C.; Perujo, A. NO_x, NH_3, N_2O and PN real driving emissions from a Euro VI heavy-duty vehicle. Impact of regulatory on-road test conditions on emissions. *Sci. Total Environ.* **2017**, *609*, 546–555. [CrossRef]
27. Commission Regulation (EU) No 582/2011 of 25 May 2011, Implementing and Amending Regulation (EC) No 595/2009 of the European Parliament and of the Council with Respect to Emissions from Heavy Duty Vehicles (Euro VI) and Amending Annexes I and III to Directive 2007/46/EC of the European Parliament and of the Council. EU COM/582/2011. Available online: https://eur-lex.europa.eu/legal-content/EN/TXT/HTML/?uri=CELEX:32011R0582&from=EN#ntr4-L_2011167FI.01008101-E0004 (accessed on 6 May 2022).

28. Van den Brink, P.J.; McDonald, C.M. Influence of the fuel hydrocarbon composition on nitric oxide conversion in 3-way catalysts: The NO_x/aromatics effect. *Appl. Catal. B Environ.* **1995**, *6*, 97–103. [CrossRef]

29. Matam, S.K.; Otal, E.H.; Aguirre, M.H.; Winkler, A.; Ulrich, A.; Ulrich, A.; Rentsch, D.; Weidenkaff, A.; Ferri, D. Thermal and chemical aging of model three-way catalyst Pd/Al2O3 and its impact on the conversion of CNG vehicle exhaust. *Catal. Today* **2012**, *184*, 237–244. [CrossRef]

30. Winkler, A.; Dimopoulos, P.; Hauert, R.; Bach, C.; Aguirre, M. Catalytic activity and aging phenomena of three-way catalysts in a compressed natural gas/gasoline powered passenger car. *Appl. Catal. B Environ.* **2008**, *84*, 162–169. [CrossRef]

31. Jääskeläinen, H. Three Way Catalysts for Methane. DieselNet Technology Guide. Revision 2017.12. Available online: https://dieselnet.com/tech/catalyst_methane_three-way.php (accessed on 21 June 2022).

32. Auvinen, P.; Nevalainen, P.; Suvanto, M.; Oliva, F.; Llamas, X.; Barciela, B.; Sippula, O.; Kinnunen, N.M. A detailed study on regeneration of SO_2 poisoned exhaust gas after-treatment catalysts: In pursuance of high durability and low methane, NH_3 and N_2O emissions of heavy-duty vehicles. *Fuel* **2021**, *291*, 120223. [CrossRef]

33. Zheng, Q.; Farrauto, R.; Deeba, M.; Valsamakis, I. Part I: A Comparative Thermal Aging Study on the Regenerability of Rh/Al2O3 and Rh/CexOy-ZrO2 as Model Catalysts for Automotive Three Way Catalysts. *Catalysts* **2015**, *5*, 1770–1796. [CrossRef]

34. Lou, D.; Ren, Y.; Li, X.; Zhang, Y.; Sun, X. Effect of Operating Conditions and TWC Parameters on Emissions Characteristics of a Stoichiometric Natural Gas Engine. *Energies* **2020**, *13*, 4905. [CrossRef]

35. Commission Regulation (EU) 2016/1718 of 20 September 2016 Amending Regulation (EU) No 582/2011 with Respect to Emissions from Heavy-Duty Vehicles as Regards the Provisions on Testing by Means of Portable Emission Measurement Systems (PEMS) and the Procedure for the Testing of the Durability of Replacement Pollution Control Devices. Available online: https://eur-lex.europa.eu/legal-content/EN/TXT/HTML/?uri=CELEX:32016R1718&from=EN (accessed on 12 May 2022).

36. Systemic. Stormossen Ab/Oy (Vaasa/Korsholm, Finland). *SYSTEMIC Circular Solutions for Biowaste.* Available online: https://systemicproject.eu/wp-content/uploads/Stormossen_fact-sheet-Associated-plants_20191003.pdf (accessed on 2 May 2022).

37. Stormossen. Annual Report 2020. Available online: https://ar2020.stormossen.fi/annual_report/vuosikertomus-2020/tulostus/ (accessed on 2 May 2022).

38. TUV. Biogas to Biomethane Technology Review. Contract Number: IEE/10/130, Deliverable Reference: Task 3.1. TUV—Vienna University of Technology. Institute of Chemical Engineering, Research Division Thermal Process Engineering and Simulation. 2012. Available online: https://www.membran.at/downloads/2012_BioRegions_BiogasUpgradingTechnologyReview_ENGLISH.pdf (accessed on 2 May 2022).

39. Ardolino, F.M.; Cardamone, G.F.; Parrillo, F.; Arena, U. Biogas-to-biomethane upgrading: A comparative review and assessment in a life cycle perspective. *Renew. Sustain. Energy Rev.* **2021**, *139*, 110588. [CrossRef]

40. Uusitalo, V.; Havukainen, J.; Manninen, K.; Höhn, J.; Lehtonen, E.; Rasi, S.; Soukka, R.; Horttanainen, M. Carbon footprint of selected biomass to biogas production chains and GHG reduction potential in transportation use. *Renew. Energy* **2014**, *66*, 90–98. [CrossRef]

41. JRC. *Well-to-Wheels Analysis of Future Automotive Fuels and Powertrains in the European Context, Well-to-Tank Report Version 4.a*; European Commission Joint Research Centre (JRC): Brussels, Belgium, January 2014. [CrossRef]

42. StatFin. Fuel Classification. Statistics Finland. 2021. Available online: https://www.stat.fi/tup/khkinv/khkaasut_polttoaineluokitus.html (accessed on 3 May 2022).

43. Majer, S.; Oehmichen, K.; Kircshmeyr, F.; Scheidl, S. *Calculation of GHG Emission Caused by Biomethane. Biosurf. Fuelling Biomethane. Deliverable 5.3*; European Union: Brussels, Belgium, 2016. [CrossRef]

44. Bauer, F.; Hulteberg, C.; Persson, T.; Tamm, D. Biogas Upgrading—Review of Commercial Technologies. Swedish Gas Technology Centre, SGC Report 2013:270. Available online: https://www.sgc.se/ckfinder/userfiles/files/SGC270.pdf (accessed on 20 May 2022).

45. EEA. Indicators. Greenhouse Gas Emission Intensity of Electricity Generation in Europe. European Environment Agency. 2021. Available online: https://www.eea.europa.eu/ims/greenhouse-gas-emission-intensity-of-1 (accessed on 2 May 2022).

46. Söderena, P.; Nylund, N.-O.; Mäkinen, R. City Bus Performance Evaluation. VTT Technical Research Centre of Finland. VTT Report No. VTT-CR-00544-19. 2019. Available online: https://cris.vtt.fi/ws/portalfiles/portal/26400446/City_bus_performance_evaluation.pdf (accessed on 10 June 2022).